REPORT DOCUMENTATION PAGE

AFRL-SR-BL-TR-98-

0141

1. AGENCY USE ONLY *(Leave blank)*	2. REPORT DATE	3. REPORT TYPE AND DATES COVERED
	14 DEC 97	FINAL REPORT 15 SEP 96 - 14 SEP 97

4. TITLE AND SUBTITLE
(DURIP-96) ACQUISITION OF LIGHT SCATTERING AND ELECTROPHORESIS EQUIPMENT FOR STUDIES ON NANOSOL SYNTHESIS AND PROCESSING FOR DEVICE FABRICATION

5. FUNDING NUMBERS
F49620-96-1-0428

3484/US
61103D

6. AUTHOR(S)
MICHAEL TSAPATSIS, DIONISIOS VLACHOS, AND ROBERT ROWELL

7. PERFORMING ORGANIZATION NAME(S) AND ADDRESS(ES)
UNIVERSITY OF MASSACHUSETTS
MUNSON HALL, BOX 36010
AMHERST, MA 01003

8. PERFORMING ORGANIZATION REPORT NUMBER

9. SPONSORING/MONITORING AGENCY NAME(S) AND ADDRESS(ES)
AIR FORCE OFFICE OF SCIENTIFIC RESEARCH (AFOSR)
110 DUNCAN AVENUE SUITE B115
BOLLING AFB DC 20332-8050

NA

10. SPONSORING/MONITORING AGENCY REPORT NUMBER

11. SUPPLEMENTARY NOTES

12a. DISTRIBUTION AVAILABILITY STATEMENT
APPROVED FOR PUBLIC RELEASE, DISTRIBUTION IS UNLIMITED

12b. DISTRIBUTION CODE

13. ABSTRACT *(Maximum 200 words)*

The DOD funds were used by the Department of Chemical Engineering and Chemistry of the University of Massachusetts for the acquisition of light scattering and electrophoresis instrumentation: 1) An electrophoresis and dynamic light scattering system for particle size and complete zeta potential/imobility measurements. 2) A light scattering system with a 2 watt Argon-ion laser and goniometer allowing rapid multiangle static and dynamic measurements for in-situ nucleation and growth studies. 3) An X-ray attenuation particle sizer for rapid particle size measruements doen to `0mm with superior resolving capacity to complement the above instrumentation. The instrumentation is fully functional and located in Geossmann Laboratory at UMass in the laboratories of the PI's and is used for studies on Nucleation and Growth of Nanoparticles and Processing of Colloidal Nanophase Suspensions for Device Fabrication. Four graduate sutdents are using the instrumentation for their PhD projects.

19980210 059

14. SUBJECT TERMS

15. NUMBER OF PAGES
43

16. PRICE CODE

17. SECURITY CLASSIFICATION OF REPORT	18. SECURITY CLASSIFICATION OF THIS PAGE	19. SECURITY CLASSIFICATION OF ABSTRACT	20. LIMITATION OF ABSTRACT
UNCLASSIFIED	UNCLASSIFIED	UNCLASSIFIED	

ACQUISITION OF LIGHT SCATTERING AND ELECTROPHORESIS EQUIPMENT FOR STUDIES ON NANOSOL SYNTHESIS AND PROCESSING FOR DEVICE FABRICATION

FINAL TECHNICAL REPORT
for grant #: F49620-96-1-0428
15 September 1996 - 14 September 1997

Submitted to
AFOSR/NA
110 Duncan Avenue Room B115
Bolling AFB DC 20332-8080

by

Michael Tsapatsis
Principal Investigator
Dept. of Chemical Engineering
(413) 545-0276

Dionisios G. Vlachos
Co-Principal Investigator
Dept. of Chemical Engineering
(413) 545-6143

Robert L. Rowell
Co-Principal Investigator
Department of Chemistry
(413) 545-0247

The University of Massachusetts, Amherst
Amherst, Massachusetts 01003

December 14, 1997

ABSTRACT

The DOD funds were used by the Departments of Chemical Engineering and Chemistry of the University of Massachusetts for the acquisition of light scattering and electrophoresis instrumentation:

- An electrophoresis and dynamic light scattering system for particle size and complete zeta potential/mobility measurements.
- A light scattering system with a 2 watt Argon-ion laser and goniometer allowing rapid multiangle static and dynamic measurements for in-situ nucleation and growth studies.
- An X-ray attenuation particle sizer for rapid particle size measurements down to 10nm with superior resolving capacity to complement the above instrumentation.

The instrumentation is fully functional and located in Goessmann Laboratory at Umass in the laboratories of the PI's and is used for studies on Nucleation and Growth of Nanoparticles and Processing of Colloidal Nanophase Suspensions for Device Fabrication. Four graduate students are using the instrumentation for their PhD projects.

LIST OF INSTRUMENTATION

The acquired equipment are as follows:

ITEM 1

			Cost
X-Ray Attenuation Particle Sizer			
BI-XDC	X-Ray Scanning Detector Software & Computer X-Ray disc centrifuge Gravitational & Centrifugal modes	list price	$50,000
BI-DSCX	Replacement disc for aqueous suspensions	list price	$1,000
BI-DSCXR	Disc for agressive solvents	list price	$2,200
		total list price	$53,200
		discount	-$5,320
		price after discount	$47,880

ITEM 2

			Cost
Zeta Plus: Electrophoresis and Dynamic Light Scattering Particle Size Analyzer			
Zeta Potential analyzer for colloidal suspensions		list price	$29,950
BI-MAS Hardware & Software for Particle Size Analysis by Dynamic Light Scattering		list price	$10,000
Upgrade to 15 mW laser		list price	$1,000
		total list price	$40,950
		discount	-$4,950
		price after discount	$36,855

ITEM 3		*Cost*
Multiangle Light Scattering System (Static & Dynamic)		
BI-9000AT Autocorrelator/Cross correlator/Signal Processor/Computer for particle size measurements	list price	$16,250
BI-25NS Additional High Speed Channels	list price	$1,500
BI-IP Printer	list price	$650
BI-CON Stepping motor controller	list price	$1,125
BI-PCS Cumulant Fit Analysis Software	list price	$350
BI-IST Alignment Software for Use with the BI-200SM Goniometer	list price	$350
BI-ISDA Size Distribution Software	list price	$1,250
BI-200SM Goniometer for light scattering measurements with PMT (Photomultiplier Tube) and Complete Detector Optics	list price	$27,000
BI-SCAHT Scattering Cell Assembly High Temperature Option	list price	$2,000
BI-LRM Mounts for Laser	list price	$1,050
BI-TCD200 Circulator for temperature control	list price	$2,795
BI-FC Filtration Circulation System for Index Matching Fluid	list price	$1,050
BI-HV High Voltage Power Supply for PMT	list price	$1,050
BI-RC 12 Sample cell	list price	$5
BI-RC 25 Sample cell	list price	$200
BI-RC 27 Sample cell	list price	$40
BI-OIST On-site installation	list price	$2,000
	total list price	$58,665
	discount	-$5,867
	price after discount	$52,798

Items 1,2 and 3 were purchased from Brookhaven Instruments Co. Total amount paid to BIC is $137,533.

ITEM 4		*Cost*
Lexel 95-2 2 Watt Argon-ion laser, water-cooled with power supply and connections	list price	$18,500
	total list price	$18,500
	discount	-$1,850
	price after discount	$16,650

Item 4 was purchased from Lexel Laser Inc.. Total amount paid was $16,650 of which $2,183 were from the NSF CAREER Award to Michael Tsapatsis. The amount paid from the DOD grant was $14,467.

The total amount paid from the DOD grant for Items 1,2,3, and 4 was $152,000 ($137,533 + $14,467) which was the total amount of the grant. Of the $152,000, $92,000 were provided by DOD and $60,000 from the University of Massachusetts. The cost sharing was distributed as follows:

School of Engineering	$10,000
Department of Chemical Engineering	$5,000
Graduate School, Office of Vice Chancellor for Research, Graduate Studies and Economic Development:	$45,000
Total	$60,000

In addition a water cooling system for the laser (ITEM 4) was purchased with funds from the Packard Foundation: split system Icewagon chiller serial no. DE4AC 9712185 total cost $8,463 (price after discount $8273 +$190 shipping).

The instrumentation is used in studies of Nucleation and Growth during hydrothermal synthesis of zeolites and other molecular sieves. It is also employed to characterize the stability of nanosols of these materials used for device fabrication. In conjunction with the above experimental efforts we have initiated a program to understand hydrothermal synthesis kinetics as well as film deposition from nanosols through detail mathematical modeling. Both continuous and stochastic models are employed. One paper has been accepted for publication and one is submitted (enclosed) acknowledging support from DOD and two more are in preparation. Progress on the research activities during 1997 is given bellow.

RESEARCH ACTIVITIES MAKING USE OF THE INSTRUMENTATION

(Support is provided by the National Science Foundation, The David and Lucile Packard Foundation, the American Chemical Society, NETI, Engelhard Co. and Amoco Chemicals)

1. Introduction

Zeolites and non aluminosilicate molecular sieves are crystalline materials with well defined pore shapes and sizes. Their porous network structure and its close connection with their macroscopic properties provide for organization, discrimination and recognition of molecules with precision that can be less than 1Å. As a result, in addition to the traditional interest that stems from their wide utilization as selective adsorbents, catalysts and ion exchangers, molecular sieves are drawing attention in all fields of molecular recognition phenomena and have potential advanced electronic, magnetic and optical applications. Recently this potential has been demonstrated with the controlled incorporation of guest compounds (semiconductor clusters, dye molecules) in zeolite lattice hosts. By choosing from the expanding list of molecular sieve hosts, the guest size and size distribution as well as host/guest interactions can be varied.

These recent advances have demonstrated the potential of molecular sieve based materials for high-density optical storage, optical switching, laser focusing and for high resolution spectroscopy. In order to transform such early visions in commercial reality several obstacles have to be overcome (ex. long range crystal order, topographic uniformity, perturbations imposed by the zeolite matrix, wave function overlap of neighboring clusters). A most important prerequisite for any future development is our ability to engineer methods allowing molecular sieve processability into thin films on appropriate substrates and device structures. These films should consist of uniform, oriented, thin, nonscattering zeolite layers.

At a different scale, molecular sieve thin films are highly desirable for the preparation of novel chemical reactors, selective chemical sensors and membranes. Molecular sieve membranes could operate continuously in separation processes under high temperature and corrosive atmospheres and can be integrated in membrane reactor configurations leading to the development of new processes unattainable with the current reactor technology. Typical examples include some selective oxidations, equilibrium limited dehydrogenations and isomerizations. Moreover, due to stability and unmatched potential for high selectivity, they provide the needed flexibility for incorporation in existing processes for valuable component recovery (ex. hydrogen recovery from petrochemical plant off-gases) and waste reduction. Unlike polymeric membranes and adsorption processes, retrofitting of existing processes can be achieved with minimal changes since cooling, reheating and pretreatment to remove components with detrimental effects to the separation process can be eliminated. Supported ultra-thin zeolite films on gauges can also find uses in the recently introduced millisecond residence time reactor configurations.

2. Research Accomplishments

It is clear that the fabrication of good quality molecular sieve films is a highly rewarding goal. To achieve this goal we are developing multi-step processing schemes.

2a. Microporous Molecular Sieve Films

The processing scheme we have developed for microporous molecular sieves is as follows:

1. Preparation of a precursor colloidal suspension of molecular sieve crystals of nanometer dimensions.

2. Deposition of a thin, oriented film (seed film) of the nanometer crystals.

3. Secondary grain growth of the deposited zeolite nanocrystals of the seed film to a continuous oriented film.

This multi-step approach allows for optimization of the individual steps and rational design of the processing scheme tailored for the specific application of the film. That flexibility consists the major advantage of the proposed scheme over the once-through, trial and error, approach of *in situ* formation. Moreover, it can overcome limitations of *in situ* preparations like device size and shape, and substrate materials, addressing the very engineering aspects of device fabrication. Although seeding in zeolite synthesis is routinely employed and it is well known that the presence of seeds on a substrate plays an important role in many thin film formation processes like, for example, diamond film formation, it was not until recently that we introduced the method of secondary growth of seed films for zeolite thin film processing. Using this method we have demonstrated, for the first time, that zeolite nucleation can be effectively decoupled from the film formation process providing an alternative route to *in situ* methods of film formation.

There are two main issues related to the development of zeolite films using secondary growth: the preparation of the precursor layer and the growth of this layer to a continuous film.

Precursor Layer Formation

Related to this issue is the preparation of colloidal suspensions of zeolite particles and their deposition procedure on the desired substrate. We applied colloidal deposition techniques for the formation of the precursor layers taking advantage of electrostatic forces between the colloidal zeolite particles in suspension and a substrate surface bearing opposite charge. Modification of the substrate by adsorption of anionic or cationic polymers as well as modification of the zeolite particles by silylation were employed (Figure 1).

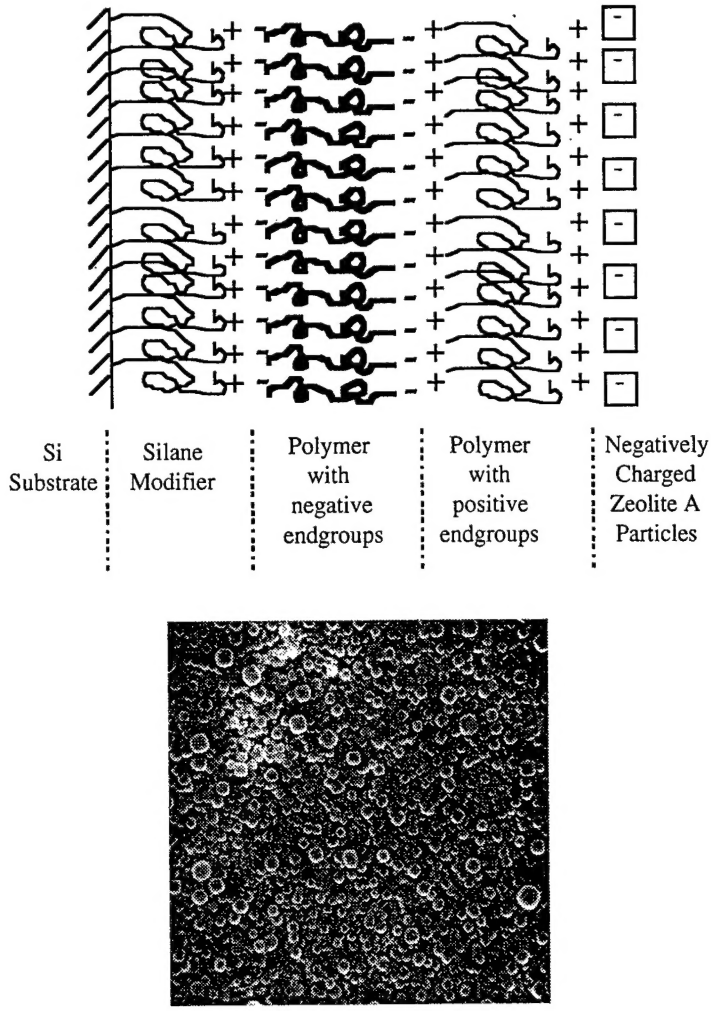

Figure 1. Deposition of zeolite A on modified silicon substrate. Schematic and top view SEM of the deposit.

Alternately, the zeolite particle suspensions can be used to deposit closely packed two dimensional colloidal crystals by convective particle transport during low speed dip coating on substrates bearing the same charge as the zeolite particles.

When the zeolite particles have an anisotropic shape then these deposition procedures can lead to oriented layers as was demonstrated by deposition of disc-shaped particles of zeolite L and cubic-shaped zeolite A particles.

In addition to particle orientation, by using convective deposition we were able to form oriented domains that span the length of several particles (Figure 2). This colloid crystal approach opens a new, elegant and efficient route for macroscopically oriented zeolite coatings based on the shape of the zeolite colloidal particles.

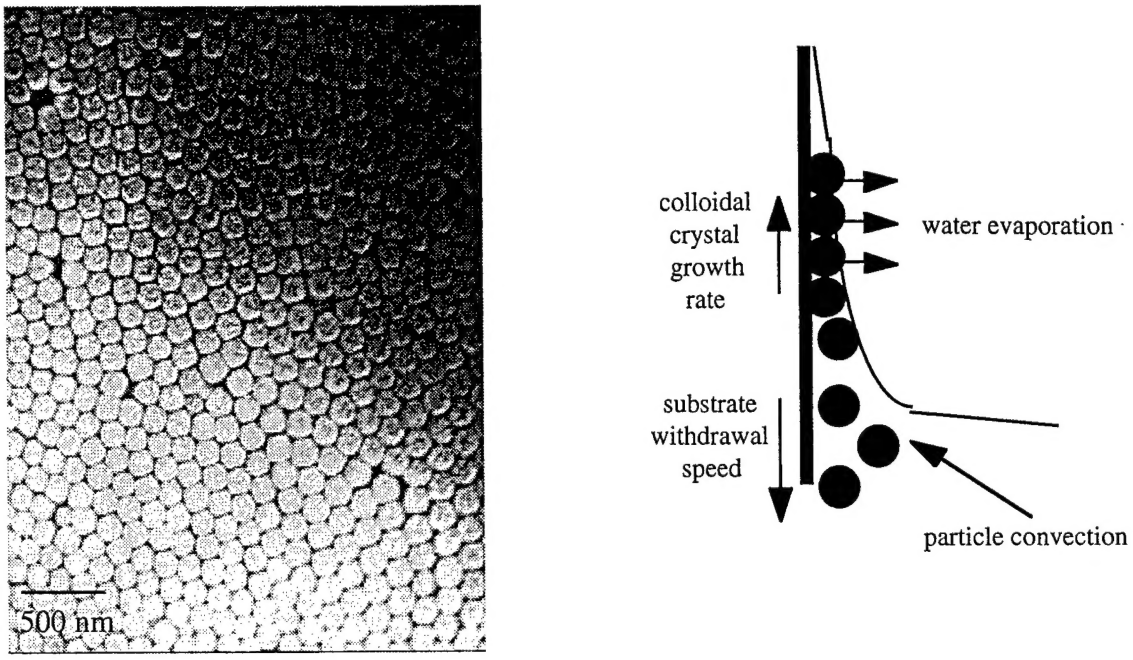

Figure 2. Formation of Colloidal Array of Zeolite Particles. Top view SEM and schematic of deposition process.

Secondary Growth

After the attachment of the precursor seed layer(s) on the substrate a secondary growth step is employed. Its purpose is the elimination of interparticle gaps by attachment of newly formed crystallites on the precursor film and/or by growth of the crystals on the precursor film.

Starting from randomly oriented nanocrystalline precursor layers we prepared continuous zeolite films. Although the precursor films are randomly oriented we identified conditions for the preparation of preferentially oriented films after secondary growth (Figure 3).

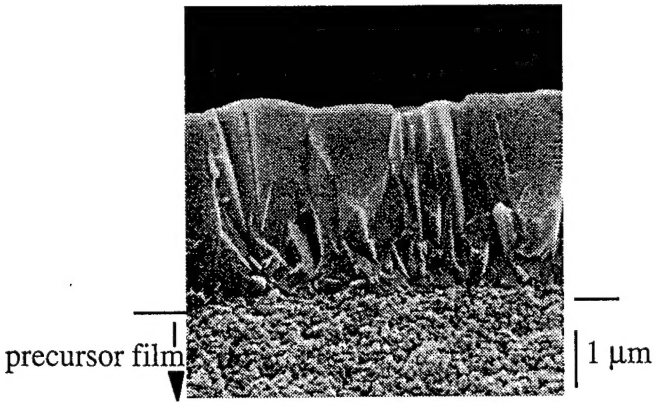

Figure 3. SEM cross section view of oriented zeolite film (structure type: MFI). Film thickness can be varied between 0.5 to 100 μm.

Due to their microstructure (film thickness, crystal orientation) these films demonstrated gas permeation and optical properties superior to previously reported MFI films prepared by *in situ* growth.

Recently, we have shown that secondary growth of precursor oriented layers of zeolite A colloid crystals leads to films which preserve the orientation of the precursor film. This demonstration provided a clear link between the orientation of the precursor layer and that of the final film.

2b. Mesoporous Molecular Sieves

A class of materials (called M41S) is extending the well defined structures of molecular sieves to the mesoporous region. Synthesis of mesoporous molecular sieves utilizes surfactants, known to form self-assembled mesostructures (micelles and lyotropic liquid crystalline phases) in aqueous solutions. The surfactant mesostructures serve as templates around which the inorganic phase is organized. We proposed that the existence of liquid crystalline mesostructures during the synthesis provides an opportunity for the development of a processing strategy similar to polymeric liquid crystals. It was suggested that an induced macroscopic ordering of the mesostructure will result in macroscopic perfection of the inorganic structure. Our work undertakes the challenge of identifying ways to induce this ordering employing flow and magnetic fields.

We have demonstrated that intergrown layers of hexagonal mesoporous silica can be deposited under continuous flow and provided evidence that the flow field can induce a preferred orientation by mechanism(s) which are independent of or in addition to substrate-

solution interfacial effects (Figure 4). That was the first time that orientation induced by an external flow field was reported for M41S type materials and may open new processing routes for film formation.

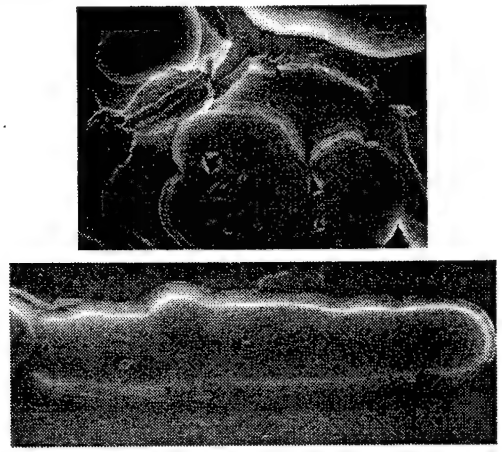

Figure 4. SEM top views of mesoporous deposits formed under static conditions (top) and flow (bottom). Magnification 25,000.

submitted

Microstructural Design for Optically Transparent and Oriented Molecular Sieve Films

Anastasios Gouzinis and Michael Tsapatsis*
Department of Chemical Engineering
University of Massachusetts Amherst, Amherst, MA 01003

The preparation of advanced materials based on molecular sieves has attracted considerable interest with target applications including optoelectronic devices, molecular sieve membranes and sensors[1]. In particular, the potential for optical applications including optical storage[1,2], tunable non-linear optical materials[3] and visible light photocatalytic coatings and membranes[4] has been demonstrated. In order to extend these demonstrated concepts to practical devices there is a need for microstructurally engineered coatings of the zeolite of choice on appropriate substrates[5-9]. Here, combined microstructural control over film thickness, surface roughness, crystal orientation, continuity and intergrowth is demonstrated for molecular sieve films of silicalite (MFI structure type) over macroscopic length scales. As a result of their microstructure exhibiting well intergrown, oriented, columnar texture with small surface roughness, films with thicknesses well exceeding the wavelength of visible light are optically transparent.

---

* Corresponding Author: tsapatsi@ecs.umass.edu

Deposition of oriented molecular sieve coatings has been demonstrated by *in situ* growth[10,11]. Despite considerable progress in developing zeolite films by *in situ* growth no preparation has been demonstrated to lead to highly oriented films, of uniform controllable thickness and a microstructure limiting visible light scattering.

In a different approach, the deposition of pre-synthesized zeolite crystals as non-bonded particulate coatings[7,12] or as composite films bonded with an index matching binder[1-3] has been proposed. In this scheme, crystal orientation is achieved by applying an electric field[3] or by making use of the zeolite particle shape[7,12]. Limitations associated with the presence of a binder such as stability and access to the zeolite interior, as well as difficulties in controlling crystal uniformity, density, packing and intercrystalline porosity of particulate films pose practical bounds to possible applications.

Translucent zeolite coatings and monoliths have also been prepared from nanocrystalline zeolite particles[5]. However, they consist of randomly oriented grains limiting their possible applications when crystal orientation is required.

A processing scheme for the preparation of molecular sieve films has been introduced recently. It consists of first preparing colloidal suspensions of zeolite particles which are then used to deposit precursor films on various substrates. Following the formation of the precursor particulate film a secondary growth step is applied during which the precursor particles grow larger to eliminate intercrystalline porosity[5-9]. It was demonstrated that under certain secondary growth conditions preferentially oriented films of MFI can be prepared from randomly oriented precursor films[6,9]. Moreover, starting from oriented precursor films of zeolite A highly oriented intergrown films of zeolite A[7]

conditions the silicalite particles are negatively charged. A similarly charged glass substrate is immersed and withdrawn from the suspension. The coated substrate is then left to dry in air at room temperature overnight followed by 2hrs drying at 50° C. During this procedure a thin nearly monolayer coating of silicalite particles is deposited on the substrate. The formation of the coating proceeds during the slow evaporation of water during which the zeolite particles remain mobile and rearrange on the surface. Eventually, the particles are attached to the surface once the water layer thickness becomes less than the particle size. Variations of such deposition techniques which do not require attraction of the particles by the substrate but rely on Brownian motion and convection of particles during solvent evaporation have been applied for the formation of latex colloidal crystals as well as ordered arrays of proteins[13].

Following the formation of the precursor layer the glass slides were placed in contact with a solution with typical composition 5x SiO_2 : x TPAOH : 10000 H_2O :20xEtOH and heated for up to several days at temperatures ranging from 90° C to 170° C under static conditions. Figure 1a-d shows SEM top-views and cross-sections at various stages during film growth at 145°C. The high density of nanocrystalline seeds with surfaces amenable to continuing growth allows for uniform deposition propagating with time as a moving front from the precursor layer to the solution at a constant rate. No induction period is observed, clearly showing that the presence of seeds (having active external surfaces) leads to elimination of the film nucleation stage. The fastest growing c-direction dominates the film texture resulting in crystal grains oriented with their c-axis perpendicular to the substrate. As a result of the high density of uniformly growing

grains even under conditions of relatively high supersaturation, pronounced surface roughening is not observed and a smooth film surface is obtained. Such uniform sustained film growth has not been reported in any of the previous studies of zeolite film growth and clearly illustrates the power and flexibility of secondary growth. Growth at lower temperatures and, consequently, lower growth rates results in even smoother surfaces (Figure 1e).

The preferred orientation of the film is verified by X-Ray diffraction using standard θ–2θ scan (Figure 2c). Additional pole-figure analysis (Figure 2d) shows a distribution of (002) planes with a half width at half maximum of 8° centered at 0° tilt. Modification of the synthesis conditions can lead to films similarly oriented with thicknesses ranging from 1μm to ~100μm[14].

The transparency of the films is illustrated in Figure 3 where the region coated with the precursor layer is contrasted with the uncoated one. After prolonged secondary growth the region of the substrate which was not coated with the precursor layer is covered with crystals nucleated during secondary growth. Incorporation of such crystals in the coated area of the substrate is not observed. This is a clear demonstration that the film growth kinetics in the two regions (coated vs. uncoated) are different.

What is the reason for the dramatic influence of the precursor layer on film growth kinetics? In the presence of the precursor layer the nucleation stage is bypassed and growth starts as soon as the particles in the precursor layer come in contact with the secondary growth solution. The uniform growth of the existing crystals, once initiated, is

self-preserved by preventing the nucleation of new crystals in the vicinity of the growing film due to the steady consumption of nutrients, precursors and extended structures able to contribute to crystal growth. Therefore, the role of the precursor layer is dual. It not only leads to growth without the need for nucleation but also prohibits the incorporation of newly formed crystals which will degrade film quality. On the basis of this observation this study provides support to the "agglomeration model" for silicalite nucleation and growth proposed by Thompson and co-workers[15]. Based on light scattering measurments, it was hypothesized that nonviable nuclei are continuously produced and upon their formation they can be incorporated to growing crystals or continue to grow to form new nuclei.

In conclusion, we have demonstrated that optically transparent oriented films of silicalite with controlled thicknesses, and grain size well exceeding the wavelength of visible light can be directly synthesized in the absence of binders and orienting external fields by uniform sustained secondary growth of seed particles. The method of preparation, although surface initiated is independent of substrate composition, shape and size[6] provided that a thin layer of precursor particles can be prepared.

To our knowledge, combined microstructural control over film thickness, uniformity, surface roughness, crystal orientation, continuity and intergrowth for molecular sieve films has not been demonstrated before. The preparation of high quality molecular sieve films will contribute in developing practical optoelectronic devices[3], optical sensors and transparent membranes for visible light photocatalysis[4] and spectroscopy.

The microstructural control demonstrated here is also of significance for the use of these films in equally important applications such as membranes for gas separations and coatings on surface acoustic wave sensors. We have prepared films of the same quality on porous alumina substrates. Permeation studies through such films with similar orientation and degree of intergrowth but variable thickness will provide information on the role of microstructure on transport properties.

Finally, further studies of the dependence of the substrate independent film growth rate on synthesis conditions should contribute in further understanding the complicated nucleation and growth processes in hydrothermal synthesis.

References

1. Ozin, G.A., Kuperman, A. & Stein, A. *Angew. Chem. Int. Edn. Engl.* 28, 359-376 (1989).

2. Stein, A. *M. Sc. Thesis, University of Toronto*, (1988).

3. Caro, J. et al. *Adv. Mater.* 4, 273-276 (1992).

4. Frei, H., Blatter, F. & Sun, H. *Chemtech.*, 24-30 (1996).

5. Lovallo, M.C., Tsapatsis, M. & Okubo, T. *Chem. Mater.* 8, 1579-1583 (1996).

6. Lovallo, M.C. & Tsapatsis, M. *AIChE J.* 42, 3020-3029 (1996).

7. Boudreau, L. & Tsapatsis, M. *Chem. Mater.* 9, 1705-1709 (1997).

8. Mintova, S. et al. *Chem. Commun.* 15-16 (1997).

9. Lai, W. et al. *International Patent Application*, WO 96/01687 (1996).

10. Feng, S. & Bein, T. *Nature* 386, 834-836 (1994).

11. Koegler, J.H., van Bekkum, H. & Jansen, J.C. *Zeolites* 19, 262-269 (1997).

12. Laine, P., Seifert, R., Giovanoli, R. & Calzaferri, G. *New J. Chem* 21, 453-460 (1997)

13. Nagayama , K. *Colloids and Surfaces* 109, 363-374 (1996).

14. Lovallo, M.C., Gouzinis, A. & Tsapatsis, M. to be submitted to *AIChE J*

15. Twomey, T.A.M., Mackay, M., Kuipers, H.P.C.E. & Thomson, R.W. *Zeolites* 14, 162-168 (1994).

ACKNOWLEDGMENT Support for this work was provided by NSF, the David and Lucile Packard Foundation, NETI and DOD(DURIP).

List of Figures

Figure 1. Film evolution during secondary growth at 145°C (a-d). The film thickness growth rate is 0.3 μm/hr and is sustained until substantial nutrient depletion (24hrs). After this point a decrease of the crystal growth rate is observed accompanied with substantial surface roughening. However, replacing the substrate in a fresh solution leads to continued growth. By repeating this procedure film thickness can be adjusted as desired. At 90°C a film thickness growth rate of 0.01 μm/hr is obtained. After the film thickness exceeds 1 μm, growth at this lower rate leads to a surface roughness which can hardly be resolved by SEM (<.01μm) as shown in Figure 1e. An apparent activation energy of 70kJ/mol for crystal growth was calculated for secondary growth between 90 and 170°C.

Figure 2. A typical film obtained after 20hrs at 145° C is shown in Figure 2. Figure 2a shows a cross section with very uniform thickness consisting of columnar grains oriented with their c-axis perpendicular to the substrate. Single grains can be traced from the surface to the bottom of the film. Surface roughness is of the order of 0.05 μm as shown in the tilted (30°) SEM view(b).

(c) X-ray diffraction pattern and (d) orientation distribution of the (002) planes as determined by pole figure analysis. A θ-2θ geometry was used for the collection of the XRD pattern in (c). In this geometry only planes nearly parallel to the film surface contribute to the XRD pattern providing evidence of preferred orientation. The (002) peak is clearly resolved at 13.2° 2θ. To quantitate the degree of orientation, pole figure analysis of the (002) peak was used (d). Defocusing correction for the pole figure shown using a randomly oriented MFI film did not lead to any quantifiable change of the orientation distribution due to its small width and centering at 0°.

Figure 3. SEM top view (a) and optical micrograph (c) from the interface of coated and uncoated part of the substrate (b) after secondary growth. As shown by SEM examination of the two regions the deposit in the uncoated area is not uniform or continuous (Figure 3a). In contrast, a very smooth film occupies the area initially covered with the precursor layer. Optical inspection of the coated part of the glass substrate after secondary growth does not reveal any difference from the as received glass slides while the uncoated part appears nearly white due to light scattering (Figure 3b,c).

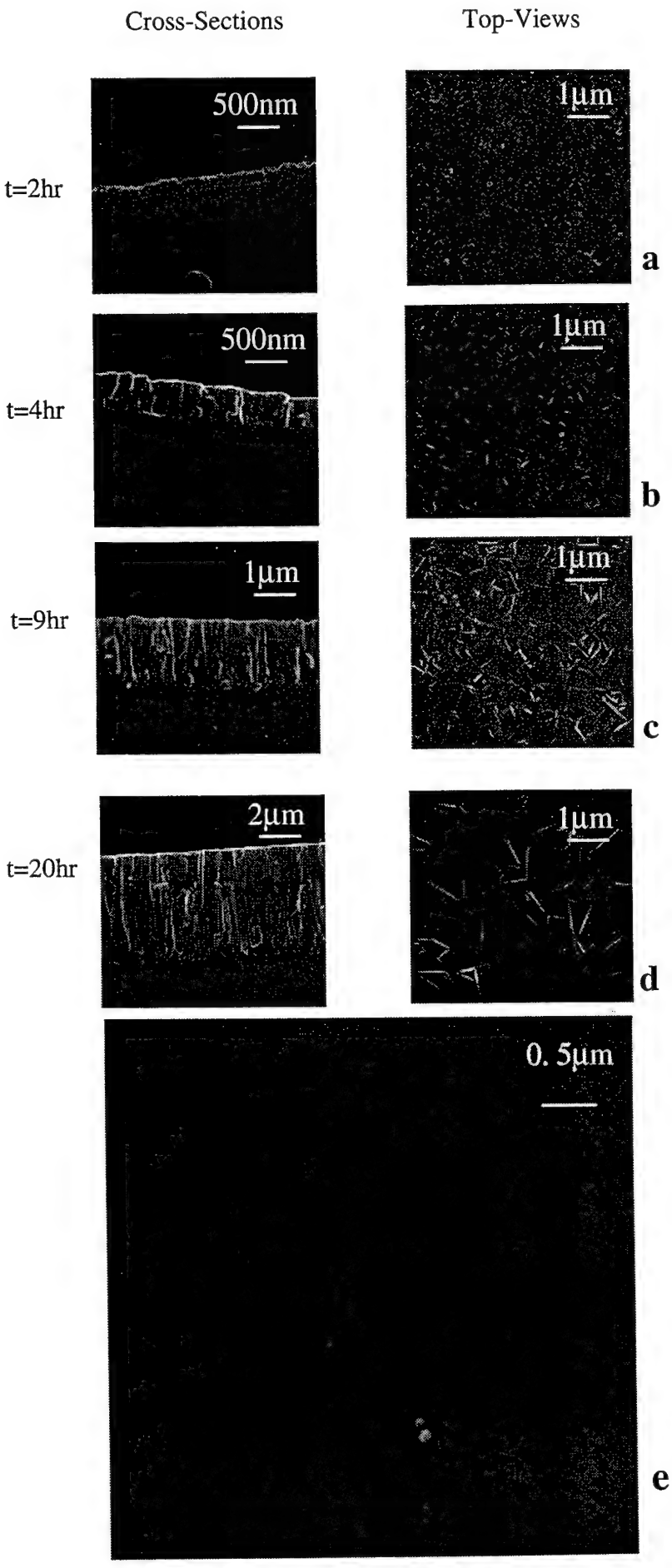
Cross-Sections
Top-Views
500nm
1μm
t=2hr
a
500nm
1μm
t=4hr
b
1μm
1μm
t=9hr
c
2μm
1μm
t=20hr
d
0. 5μm
e

Figure 1

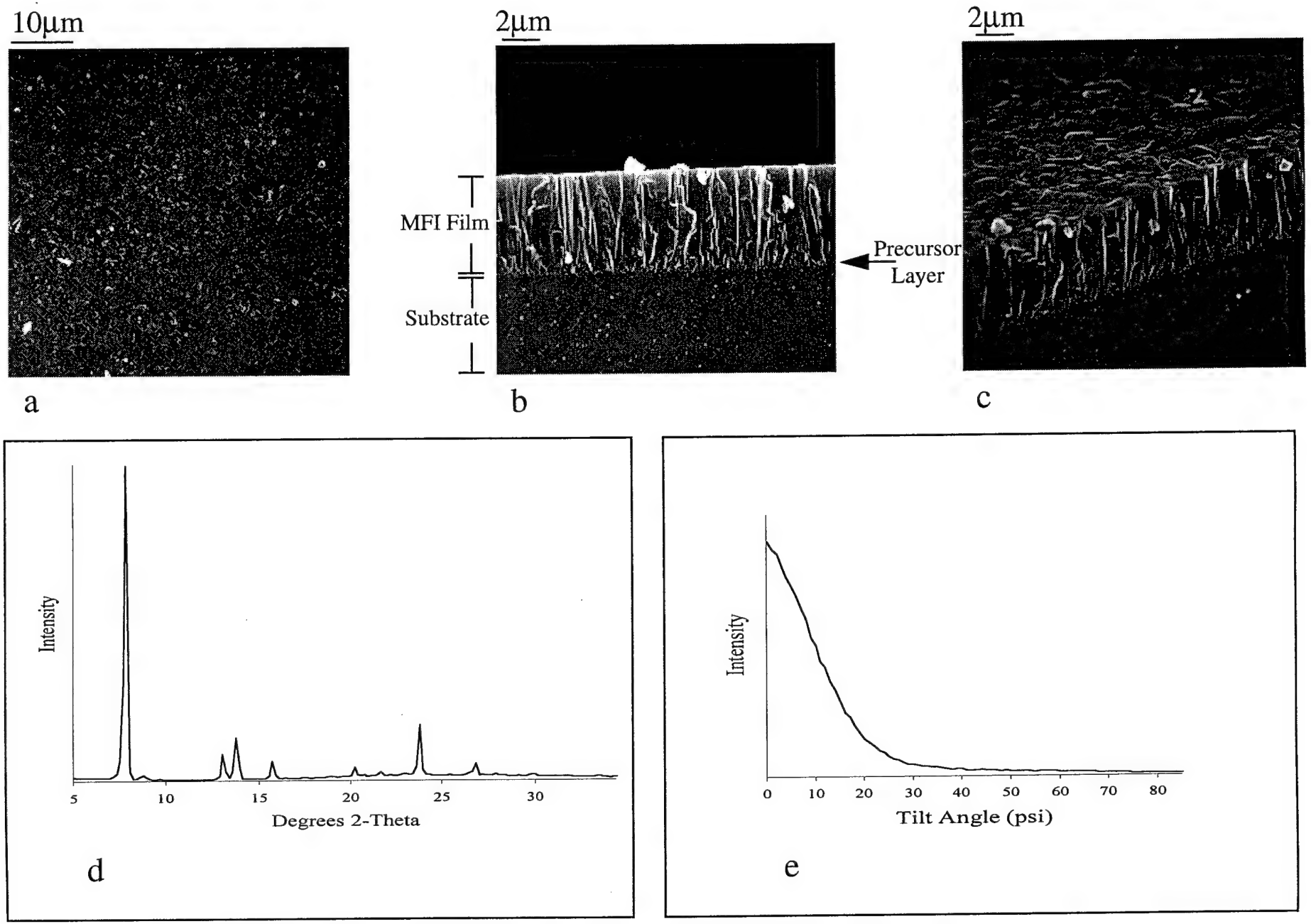
10μm
2μm
2μm
MFI Film
Substrate
Precursor Layer
a
b
c
Intensity
5
10
15
20
25
30
Degrees 2-Theta
d
Intensity
0
10
20
30
40
50
60
70
80
Tilt Angle (psi)
e

Figure 2

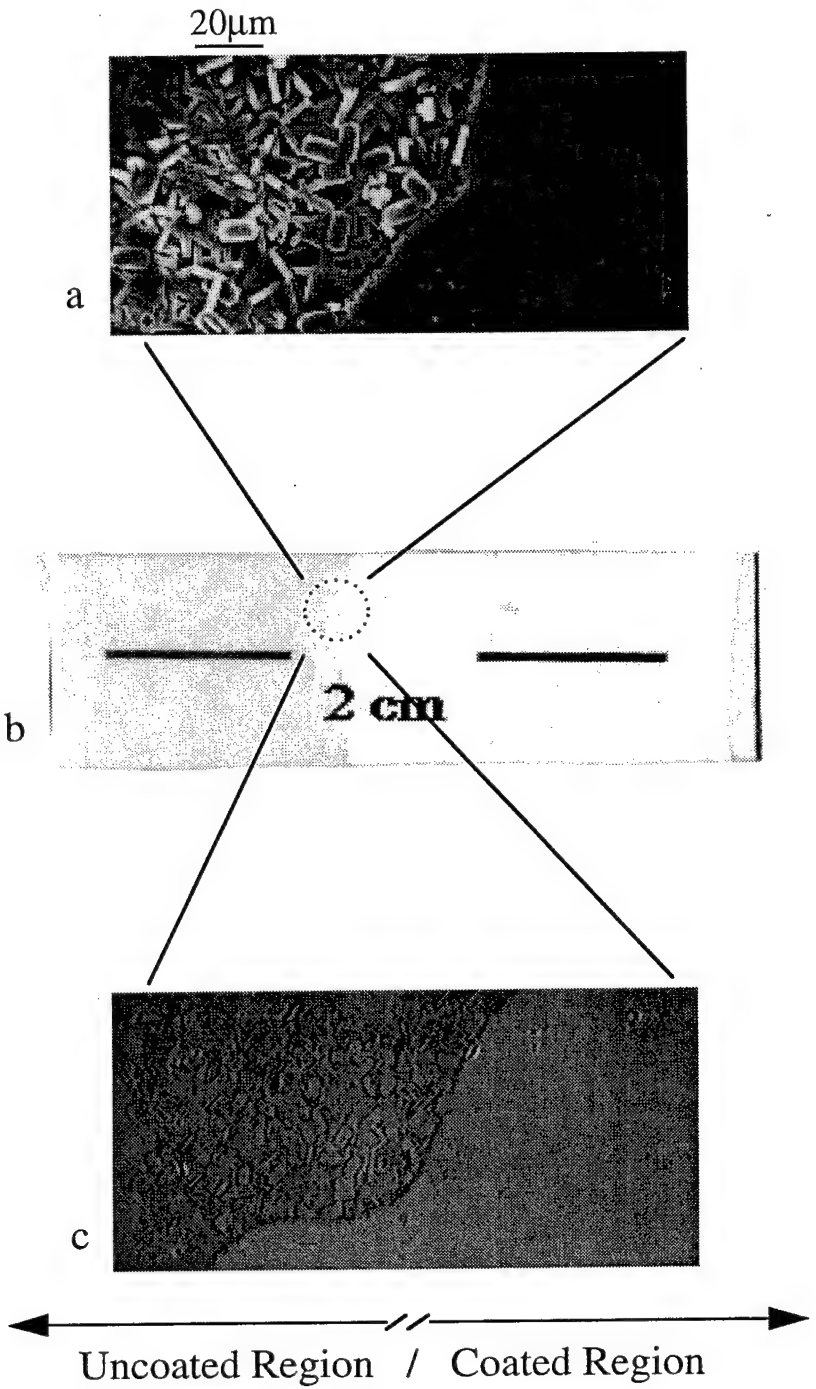

Figure 3

to appear in Microporous Materials

MODELING OF ZEOLITE CRYSTALLIZATION: THE ROLE OF GEL MICROSTRUCUTRE

Vladimiros Nikolakis, Dionisios G. Vlachos, and Michael Tsapatsis
Department of Chemical Engineering,
University of Massachusetts Amherst,
Amherst, MA 01003

ABSTRACT

The population balance formulation has been employed in order to describe zeolite nucleation and growth from precursor gels. Emphasis is given on the role of gel microstructure in crystallization kinetics. Gel dissolution and nucleation are treated as interfacial phenomena taking place at the boundary of the amorphous solid gel and the surrounding solution. The random capillary model was used to describe the gel structure and its evolution. The simulation results capture the essential features of zeolite crystallization phenomenology and are in qualitative agreement with experimental results. The often observed maximum in the nucleation rate at the early stages of gel to zeolite transformation under constant supersaturation is attributed to the increasing interfacial area during gel dissolution. Changes in the kinetic parameters (e.g. nucleation rate constant) considerably affect the overall crystallization kinetics and the final particle size distribution. Variation of the gel microstructure can have the same order of magnitude effects on the overall crystallization kinetics.

INTRODUCTION

The qualitative features of zeolite crystal growth from precursor gels are well established and schematically illustrated in Figure 1. The crystal growth curve represents the percentage of crystalline zeolite in the solid product as determined by x-ray diffraction(XRD). The shape of this curve very often suggests an increasing nucleation rate during crystallization [1, 2]. The nucleation rate profile, sketched in Figure 1, is not directly measured but extracted from the zeolite particle size distribution (PSD) and the linear crystal growth rate of zeolite crystals [3, 4]. In this respect a nucleus is considered to be a particle exceeding a critical size, after which the linear crystal growth rate, as determined by following the size of large crystals, is valid. Nucleation rate profiles estimated by this procedure typically show an initial period during which no appreciable nucleation takes place followed by an increasing nucleation rate period. Finally, as significant zeolite crystal growth takes place, the nucleation rate passes through a maximum after which the nucleation rate decreases.

Considerable effort has been devoted to developing mathematical models of zeolite nucleation and growth that are able to predict the features mentioned above and in particular the "autocatalytic", increasing, nucleation rate at the beginning of nucleation. The population balance models developed by Thompson and co-workers [5, 6] suggest the increasing supersaturation as a possible reason for the increase in the nucleation rate. However, the results of Budd et al. [3] , as well as those of others [1, 4] suggest that appreciable nucleation rates are observed and increase after the solution-phase concentration reaches a steady-state value. Subotic and co-workers [1], formulated a mathematical model describing nucleation by the release of nuclei from the dissolving gel. Thompson and co-workers using population balance analysis [5] provided more detail models for the above mechanism [6]. Their simulation results [6] showed an increase in nucleation rate to take place well inside the crystal growth curve in disagreement with experimental observations which show the increase to start before significant crystal growth and gel consumption [6, 7]. Gauthier et al. [8] modified the autocatalytic nucleation mechanism using an empirical non uniform distribution of nuclei in the gel. Better agreement with experimental results can be obtained as shown by Sheikh et al. [9]. However, as pointed out by these authors the concept of non uniform distribution of nuclei needs further consideration.

In the mathematical models mentioned above, gel dissolution and nucleation (in the autocatalytic formulations) are treated as functions of the total amount of gel present in the crystallizer. However, gel dissolution and nucleation are interfacial phenomena taking place at the interface between amorphous gel and solution. We have recently introduced

models of zeolite nucleation and growth which take into account the precursor gel microstructure [10]. The simulations indicated a strong influence of the gel microstructure on the apparent crystallization kinetics and suggested the increase of the interfacial area during dissolution as a possible contributor to the increasing nucleation rate under constant supersaturation.

Here, the gel microstructure model is incorporated in a population balance model and results are presented for heterogeneous nucleation kinetics involving nuclei formation at the interface of gel and solution.

CONTINUUM MODEL

THE PHYSICAL MODEL

The mathematical model that follows is based on the physical picture shown in Figure 2. The precursor gel is an hierarchical structure involving micro, meso, and macropores. Zeolite nucleation takes place at the interface between the solution and the gel by adsorption and rearrangement of the soluble precursors. This picture of heterogeneous nucleation is based on the consideration that at the interface there is abundance of precursors which can rearrange before their release in solution. We consider that homogeneous nucleation in the solution phase does not take place as suggested by Bronic and Subotic based on calculations using classical nucleation theory [11] and pointed by Sheikh et al. [9] based on the heterogeneous nature of the system and population balance modeling results.

Depending on the preparation method (precursor concentrations and sources, order of mixing, etc.) the precursor gel can vary from a homogeneous nearly transparent gel spanning the crystallizer volume [12] to a particulate precipitate. However, electron microscopy studies of aluminosilicate gels [13, 14] suggest a general picture such as that shown in Figure 2. It is expected that different pore sizes will not contribute equally to the nucleation and crystal growth.

First, since in order for crystal growth to occur in a way similar to that of large crystals the nucleus needs to exceed a certain critical size, it is expected that pores which are too small to accommodate a zeolite nucleus will not contribute to the surface catalyzed heterogeneous nucleation. SAXS, Cryo-TEM and HRTEM point to sizes of precursor entities of the order of 50-100 Å [15, 16], providing a lower limit for the pore size of *active porosity* involved in nucleation and growth.

Second, large pores, especially those exceeding several microns are expected to play a minor role in interfacial nucleation due to their small surface area as compared with that of the mesopores. Therefore, the relevant interfacial area appears to be that

corresponding to pores larger than the nucleus critical size but not by far exceeding this size.

After a nucleus exceeding the critical size has been formed, it continues to grow with a size independent linear crystal growth rate by a solution mediated mechanism for crystal growth [17, 18]. Nucleation and crystal growth consume solution species while replenishment of the consumed solution species is provided by gel dissolution, which is also considered to be an interfacial process.

It is assumed that the solution phase concentration is uniform throughout the volume of the crystallizer, i.e., there is no diffusional control for transport of dissolved species throughout the gel. As a result, no concentration gradients exist between various locations of the crystallizer. Moreover, a uniform composition of the solid gel phase is implied and internal gel rearrangements, for reasons other than nucleation and growth, are neglected by assuming that these rearrangements (like Ostwald ripening by dissolution-redeposition) take place at longer time scales.

With this physical picture in mind, the formulation of the mathematical model is presented in the next section.

MATHEMATICAL MODEL FORMULATION

The precursor gel microstructure is treated as two phases with constant mass density: the solid amorphous gel, of volume fraction ε_g with molar density of nutrients υ', and the surrounding liquid, of volume fraction ε_p and a nutrient concentration G^*/ε_p, where G^* is the nutrient concentration per unit volume of the crystallizing mixture. In the absence of nuclei and crystals of course $\varepsilon_g+\varepsilon_p=1$. Following the discussion in the previous section, pores which are too small to accommodate a zeolite nucleus are ascribed to the solid gel.

The gel microstructure is modeled using the random capillary model [19]. The random capillary model uses randomly placed infinitely long capillaries to represent the pore structure and provides relations for the pore volume and surface area [19, 20]. If r is the velocity with which a solid gel surface element recedes owing to dissolution, then the consumption rate of the gel is given by:

$$\frac{d\varepsilon_g}{dt} = -4\pi\varepsilon_g B_1 r\left[1-\frac{B_0}{2\pi B_1^2}\ln\left(\frac{\varepsilon_g}{\varepsilon_{go}}\right)\right]^{1/2}, \qquad (1)$$

where ε_{go} is the initial fraction of the solid gel. B_1 and B_0 are parameters of the initial gel pore structure. For a discrete pore size distribution

$$B_o = \sum \lambda_i \tag{2}$$

$$B_1 = \sum \lambda_i R_{io}, \tag{3}$$

where λ_i is the surface density of intersections of the axes of capillaries with radius R_{io} with a fixed plane. B_0 and B_1 are the only two parameters needed to describe the pore structure and are evaluated, once the initial pore size distribution is defined, according to references [19] and [20]. The velocity of the solid gel-solution interface, r, is a function of the undersaturation and here is simply taken to be proportional to it:

$$\frac{dq}{dt} = r = k_2 v' \left(G_{eq}^{*gel} - \frac{G^*}{\varepsilon_p} \right), \tag{4}$$

where G_{eq}^{*gel} is the equilibrium solution concentration for the gel, k_2 is the gel dissolution rate constant, and q is the length over which the interface has moved due to the dissolution. At t=0, q=0.

The interfacial surface area is provided by the relation:

$$S(q) = 4\pi\varepsilon_g (B_1 + qB_o). \tag{5}$$

The random capillary model has been extensively used to describe reactions in porous media including Chemical Vapor Deposition [21] and coal combustion [19]. It can capture the fact that the interfacial area of a porous medium and its surrounding fluid (under certain conditions) can pass through a maximum during dissolution. It turns out that this is an important aspect in the crystallization process as indicated bellow.

The random capillary model is not appropriate to describe solids with large porosities, and it cannot account for loss of connectivity and fragmentation of the pore medium. However, these limitations are not prohibitive here in view of the uncertainties and hypotheses described in the previous section. First, although the total porosity of a precursor gel in a zeolite synthesis, as determined by, for example, centrifugation, can be higher than 50%, the active porosity that determines the relevant interfacial area corresponding to pores larger than the nucleus size but not exceeding by far this size, is a

small fraction of this total porosity, according to the arguments presented in the previous section. Second, loss of connectivity and gel fractionation take place later in the crystallization process when high conversions are reached and are not expected to play a dominant role at the initial part associated with zeolite nucleation.

The problem of nucleation and growth of crystals can be described by considering population balance equations [5]. This approach leads to a two variable partial differential equation which is difficult to solve. It is easier to describe crystallization by transforming the population balance to the moments of distribution. The zeroth moment, m_o, describes the number of zeolite particles, the first moment, m_1, the length of zeolite particles, the second moment, m_2, the surface area of the zeolite particles, and the third moment, m_3, the crystal volume according to:

$$\frac{dm_o}{dt} = B(t) \tag{6}$$

$$\frac{dm_1}{dt} = Qm_o \tag{7}$$

$$\frac{dm_2}{dt} = 2Qm_1 \tag{8}$$

$$\frac{dm_3}{dt} = 3Qm_2. \tag{9}$$

In order to solve these equations expressions for the crystal growth and nucleation are needed. The crystal growth is assumed to be linear with respect to the driving force and independent of the crystal size [17, 18]

$$Q = k_1 \upsilon \left(\frac{G^*}{e_p} - G_{eq}^{*zeol} \right), \tag{10}$$

where G_{eq}^{*zeol} is the zeolite equilibrium concentration, k_1 is the linear crystal growth rate constant, and υ is the zeolite molar density.

The nucleation rate is assumed to be proportional to the gel surface area and to the first power of the supersaturation:

$$B(t) = k_3 \left[G^* / \varepsilon_p - G_{eq}^{*zeol} \right] 4\pi\varepsilon_g (B_1 + B_o q), \tag{11}$$

where k_3 is the nucleation rate constant.

In order to calculate the supersaturation, a total mass balance is used. In particular, the nutrients of the solution are supplied from the gel and are consumed in nucleation and growth of the crystals. Thus,

$$\frac{d(G^* / \varepsilon_p)}{dt} = -\frac{1}{\varepsilon_p v'}\frac{d\varepsilon_g}{dt}\left(1-\frac{G^* v'}{\varepsilon_p}\right) - \frac{n}{\varepsilon_p}\frac{dm_o}{dt}\left(1-\frac{G^* v}{\varepsilon_p}\right) - \frac{1}{\varepsilon_p u}\frac{dm_3}{dt}\left(1-\frac{G^* v}{\varepsilon_p}\right), \quad (12)$$

where n, is the number of moles per nucleus.

In order to obtain the particle size distribution, an infinite number of moments is needed. An approximate distribution can be recovered from a finite number of moments by assuming the form of the distribution and using some terms of Laguerre polynomials [22]. The particle size distribution is assumed to be described by the gamma distribution, the parameters of which are estimated using m_o, m_1, and m_2:

$$n(L,t) = \frac{(\kappa/\alpha)(\kappa L/\alpha)^{\kappa-1} e^{-\kappa L/\alpha}}{(\kappa-1)!} m_o, \quad (13)$$

where n(L,t) is the number density function,

$$\alpha = m_1 / m_0 \quad (14)$$

and

$$\kappa = \frac{\alpha^2}{m_2/m_0 - \alpha^2} \quad (15)$$

The above Eqs. 1-12 were solved using a Runge Kutta method in Mathematica.

RESULTS AND DISCUSSION

Table 1 gives the parameter values used for the simulation which gave the computational results shown in Figure 3. Figure 3a shows the calculated crystal growth curve corresponding to the crystallinity determined by XRD, along with the nucleation rate profile. The crystal growth curve follows the typical sigmoidal shape while the nucleation rate profile passes through a maximum. The increase in the nucleation rate takes place early on in the crystallization process while only a small fraction (~30%) of the gel has been converted to zeolite as shown in Figure 3b. Moreover, as seen in Figure 3b the nutrient

concentration in the solution is constant during the period over which the nucleation rate increases. In fact, the nutrient concentration attains a steady-state value once the simulation is started independently of the initial concentration used. When substantial crystal growth had occurred, the supersaturation then diminishes with time. These qualitative features of the simulation results are in agreement with experimental observations (see for example [3], [8]) as discussed in the introduction. The reason for the increase in the nucleation rate is the increase in interfacial surface area, as shown in Figure 3c where the normalized nucleation rate profile is plotted along with the normalized interfacial surface area (normalization is done using the corresponding maximum value). These simulation results suggest that the increase in the nucleation rate under constant supersaturation at the early stages of zeolite crystallization from precursor gels can be partly due to a heterogeneous, solid-gel surface catalyzed nucleation mechanism accompanied with an increase of the interfacial surface area involved. It is also noted that the nucleation rate profile shows an initial low constant value which increases later in the crystallization process suggesting that the prenucleation period can be partly explained with this model formulation. It is emphasized that the use of the interfacial area and not the total amount of gel present is essential for the model predictions showing an increasing nucleation rate under constant supersaturation.

For the parameter values used in the simulations of Figure 3, gel dissolution is much faster than nucleation and growth and therefore, the steady-state supersaturation value attained is close to the equilibrium value for the gel.

It is noted again that in these simulations the nucleation rate is taken to be proportional to the interfacial surface area and the nutrients concentration in solution. That functional dependence corresponds to a surface catalyzed heterogeneous nucleation taking place by sequential addition of nutrients from solution in a manner similar to enzyme catalyzed polymerization reactions [23]. Since the supersaturation is sustained constant at a certain steady-state value for most of the crystallization process, the nucleation expression, despite its detailed functional dependence on the supersaturation, may describe as well another form of nucleation rate dependent only on the surface area of the gel. Such an expression could correspond, for example, to an autocatalytic nucleation mechanism as the one suggested by Subotic and coworkers [1], according to which the dissolving gel releases crystal precursor species during its dissolution. With this observation, as well as simulation results presented elsewhere [10], it is shown that in the framework of this phenomenological mathematical model, a mechanism involving release of nuclei from the gel cannot be clearly differentiated from a surface catalyzed heterogeneous mechanism under conditions of constant supersaturation. This is due to a general limitation involving

phenomenological descriptions. Due to the blurring of microscopic detail involved in the expressions used, more than one microscopic mechanism can be accounted for simultaneously.

In Figure 4 the effect of the nucleation rate constant k_3 is shown. It is found that the supersaturation attains the same-steady state value for all values of the nucleation rate constant but for the highest one, where the relative rate of gel dissolution becomes smaller. As the nucleation rate increases, the overall crystal growth time is reduced, as shown in panel c and the crystal size decreases as shown in panel e.

Figure 5 illustrates the effect of the gel microstructure on apparent nucleation and crystal growth kinetics. Figure 5f shows three different hypothetical pore size distributions of the precursor gel. In these simulations mesoporous precursor gels are used which describe well only a fraction of zeolite precursor systems, as for example the one formed after mixing and heating the precursor potassium silicate and aluminate in some syntheses of zeolite L nanoparticles [14]. However, the qualitative features of the model are relevant to most zeolite syntheses from precursor gels since, as argued before, the active porosity has pore sizes of the order of magnitude of the zeolite nucleus critical size. A 50% total porosity is used which is distributed differently in the three gels examined. The nucleus critical size is considered to be 7 nm, and only pores larger than this size are accounted for the interfacial surface area contributing to dissolution and nucleation. These pores constitute the active porosity indicated in Figure 5 for three distributions. The rest of the pores are ascribed to the solid gel.

As seen in Figure 5, even though the steady-state supersaturation value is not affected there is a decrease in the maximum nucleation rate as the active porosity decreases due to the decrease of the interfacial area available for nucleation. The overall time for the gel to zeolite transformation decreases with the increase of the active porosity and that is accompanied with a shortening of the tail of the nucleation rate profile. However, the crystal size is not affected much with changes in the gel microstructure; only a relative small increase in the size is observed with a decrease of the active porosity due to a corresponding decrease of the overall (apparent) nucleation rate. The difference between the initial and maximum nucleation rate becomes more pronounced with decreasing active porosity. This is due to the most pronounced maximum of the surface area for the lower initial active porosity as predicted from the random capillary model.

Figure 5 indicates that small changes in the precursor gel microstructure can have a pronounced effect on the observed nucleation and growth kinetics. Effects on nucleation rates and induction period can be as important as order of magnitude changes on rate constants such as the nucleation rate constant examined above.

The structures that have been examined above correspond to gels where the active porosity is only a small fraction of the total one. In Figure 6b simulation results from another hypothetical gel structure, that corresponds to a large fraction of the porosity present as active porosity, are compared with ones from a gel of the previous case. The pore size distributions are shown in Figure 6a. The random pore model does not predict a maximum in the interfacial area during dissolution, and as expected, the population balance model does not show a maximum in the nucleation rate under constant supersaturation. Gels with large microporosity have not been examined in more detail because their microstructure corresponds to a gel with a wide distribution of randomly placed pores rather than a hierarchical gel pore structure which is the thesis of this report (see Figure 2).

The gel microstructure hypothesized here needs to be supported from experimental data. This is a demanding task given the difficulties characterizing the wide range of length scales involved. To our knowledge, no detailed quantitative information exists on zeolite precursor gel microstuctures. Dokter et al. [24]used SANS to follow the evolution of the interfacial surface area during crystallization of silicalite from a precursor gel. Their results show a maximum in the interfacial surface area to take place before considerable transformation of the gel to zeolite and are in good agreement with the model presented here.

In the model presented and analyzed above, a lumped solution concentration was used. It is straightforward to extend this model by including balances of the individual species as well as more detailed expressions for nucleation and dependence of crystal growth on solution concentrations as those suggested by Lechert and Kacirek [25, 26]. However, it should be noted that such expressions were derived with the inherent assumption that the differences in composition of the precursor mixtures do not significantly perturb the precursor gel microstructure to affect the apparent crystallization kinetics.

CONCLUSIONS

The population balance model, with the introduction of a description of the gel microstructure, can capture the phenomenology of zeolite crystallization. The results are in qualitative agreement with experimental ones giving an explanation to the constant concentration of nutrients and to the maximum in the nucleation rate. The gel microstructure can play an important role by defining the interfacial area between the gel and the solution. For certain gel pore structures , the interfacial area passes through a maximum, causing the nucleation rate to pass also through a maximum. Small variations in gel microstructure can cause changes in the overall crystallization kinetics of the same order of magnitude with

changes caused by variations in the kinetic parameters. For quantitative predictions further improvements have to be made by including detailed chemistry in the model and by developing more detailed microstructural models.

ACKNOWLEDGMENTS

We acknowledge instrumentation support from the National Science Foundation (CTS-9410994) and the Department of Defense (DURIP). D.G.V. and M.T. acknowledge support from the National Science Foundation (CAREER, CTS-.9702615 and CAREER,CTS-9512485). M.T. is grateful to the David and Lucille Packard Foundation for a Fellowship in Science and Engineering.

REFERENCES

1. Subotic, B., and Graovac, A., *Stud.Surf.Sci.Cat.* 24:199 (1985).
2. Ciric, J., *J.Coll. Interface* 28:315 (1968).
3. Budd, P. M., Myatt,G.J., Price, C., and Carr, S.W., *Zeolites* 14:198 (1994).
4. Chen, W. H., Hu H.C., and Lee,T.Y., *Chem.Eng.Sci.* 48:3683 (1993).
5. Warzywoda, J., Thompson, R.W., *Zeolites* 9:341 (1989).
6. Thompson, R. W., Dyer, A., *Zeolites* 5:292 (1985).
7. Myatt, G. J., Budd,P.M., Price,C., Hollway,F., Carr, S.W., *Zeolites* 14:190 (1994).
8. Gonthier, S., Gova,L., Guray,I., and Thompson, R.W., *Zeolites* 13:414 (1993).
9. Sheikh, A. Y., Jones, A.G., Graham,P., *Zeolites* 16:164 (1996).
10. Tsapatsis, M., Vlachos, D.G., *MRS Symp. Proc.* (R. F. Lobo, Beck J.S., Suib S.L., Corbin D.R., Davis M.E., Iton L.E., and Zones S.I., ed.), Vol. 431, p. 197, San Francisco, CA, 1996.
11. Bronic, J., and Subotic, B., *Microporous Materials* 4:239 (1995).
12. Tsapatsis, M., Lovallo,M., Okubo,T., Davis,M.E., and Sadakata,M., *Chemistry of Materials* 7:1734 (1995).
13. Kerch, H. M., Gerhadt,R.A., Grazul,J.L., *J. Am. Ceram. Soc.* 73:2228 (1990).
14. Tsapatsis, M., Lovallo, M., and Davis,M.E., *Microporous Materials* 5:381 (1996).
15. Itoh, L. E., Trouw,F., Brun,T.O., Epperson,J.E., White J.W.,and Henderson S.J., *Langmuir* 8:1045 (1992).
16. Dokter, W. H., Van Garderen, H.F., Beelen, T.P.H., Van Santen,R.A., and Bras W., *Angew.Chem.Int.Ed. Engl.* 34:73 (1995).

17. Kerr, G. T., *J Phys Chem* 70:1047 (1966).
18. Kerr, G. T., *Zeolites* 9:451 (1989).
19. Gavalas, G. R., *AIChE J.* 26:577 (1980).
20. Sahimi, M., G.R.Gavalas, and T.T. Tsotsis, *Chem. Eng. Sci.* 45:1443 (1990).
21. Tsapatsis, M., and G.R. Gavalas, *AIChE J.* 38:847 (1992).
22. Hulburt, H. M., and Katz,S., *Chem.Eng.Sci.* 19:555 (1964).
23. Allan, F., *Enzyme Structure and Mechanism*, Freeman and Co., 1985.
24. Dokter W.H., B. T. M. P., van Garderen H.F., Rummens C.P.J., van Santen R.A., and Ramsay J.D.F., *Colloids Surfaces A: Physicochem. Eng. Aspects* 85:89 (1994).
25. Lechert H., and Kacirek H., *Zeolites* 13:192 (1993).
26. Lechert, H., *Zeolites* 17:473 (1996).

TABLE I: Values of parameters used for the simulations of Figure 3.

k_1	$3.2\ 10^{-8}$ m s^{-1}
k_2	$1.3\ 10^{-7}$ m/s^{-1}
k_3	$2.7\ 10^{5}$ m #mol^{-1} s^{-1}
G_{eq} of gel	218 mol m^{-3}
G_{eq} of zeolite	185 mol m^{-3}
Bidisperse pore size distribution with	
Total porosity	50%
Aver. micropore size= 3.28nm , 90% of total porosity	
Aver. macropore size =36.8nm , 10% of total porosity	
Calculated active porosity	9%
Calculated B_0	$7.1\ 10^{13}$ # m^{-2}
Calculated B_1	$8.0\ 10^{5}$ m^{-1}
Nucleus size	7 nm
v	$2.9\ 10^{-5}$ m^3 mol^{-1}
v'	$1.3\ 10^{-4}$ m^3 mol^{-1}

LIST OF FIGURES

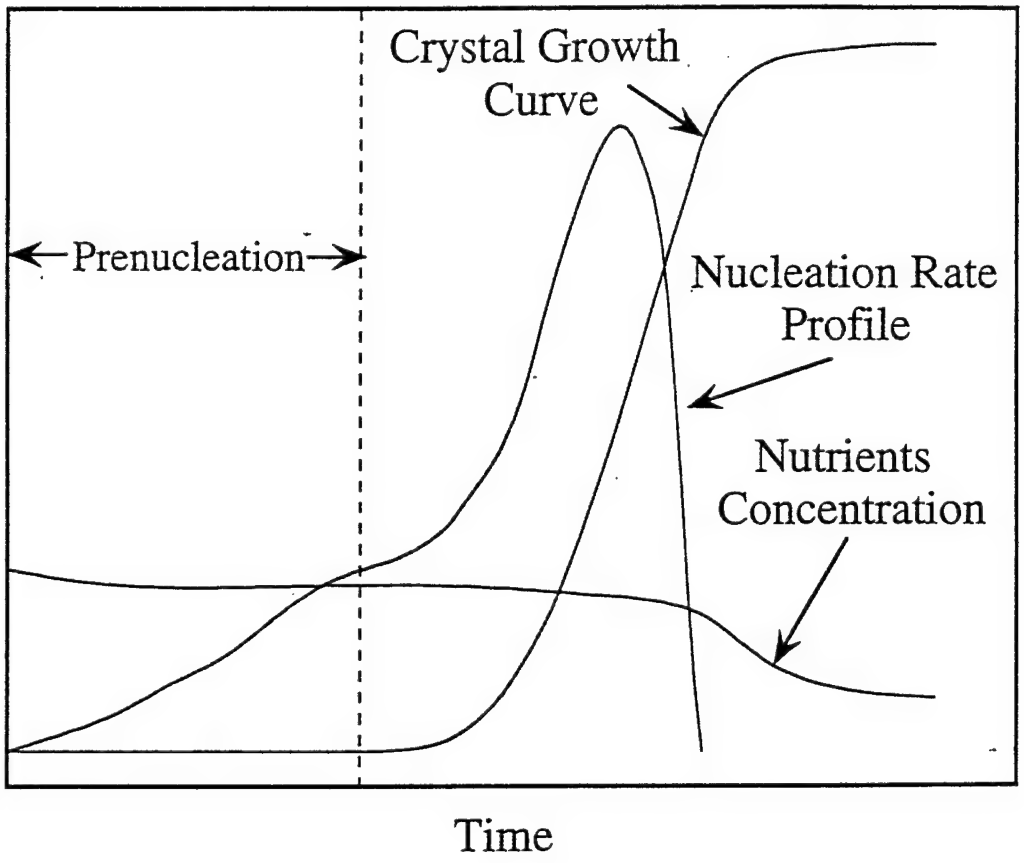

Fig. 1, Nikolakis et al.

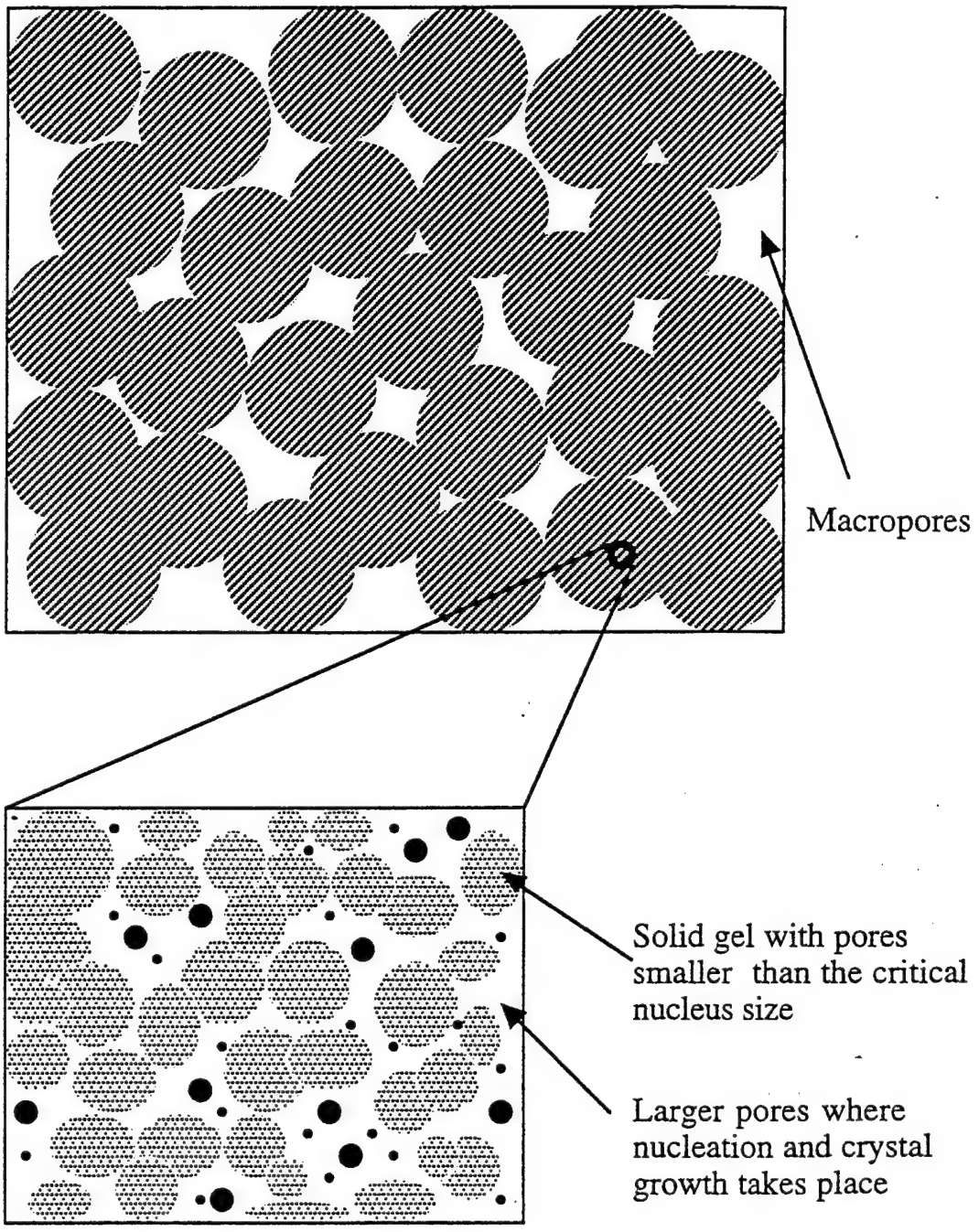

Nikolakis et al., Figure 2

Fig. 3, Nikolakis et al.

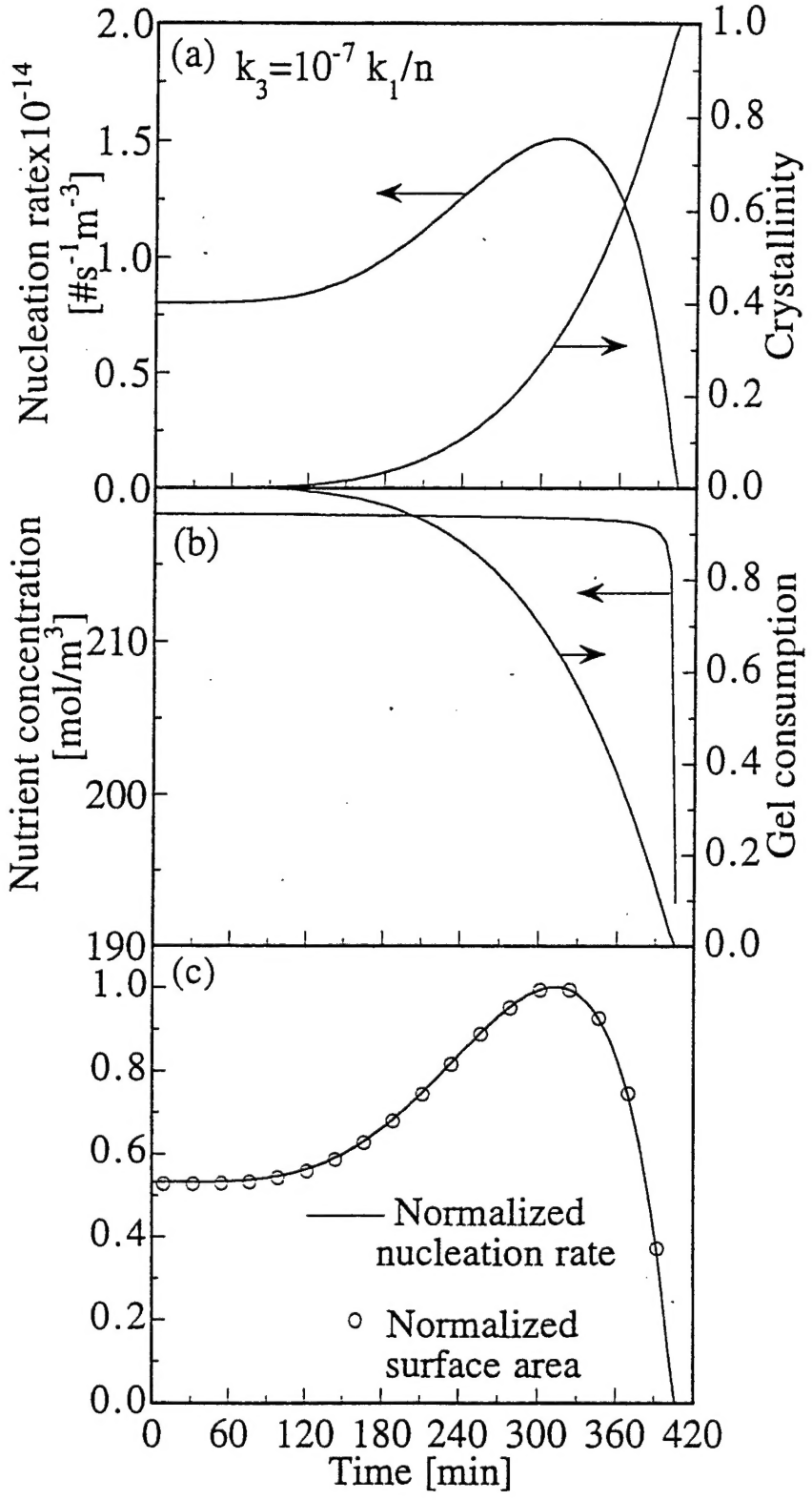

Fig. 4, Nikolakis et al.

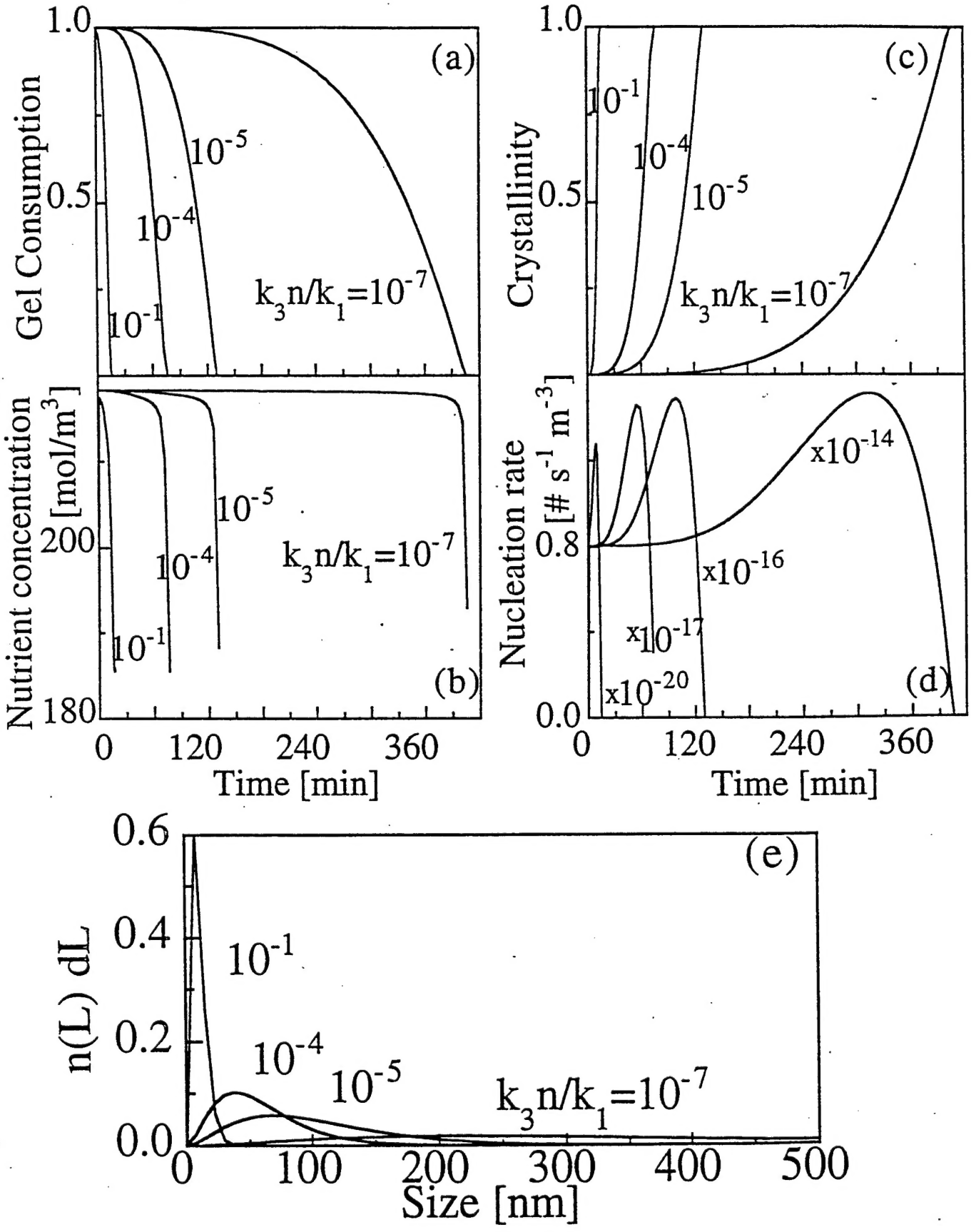

Fig. 5, Nikolakis et al.

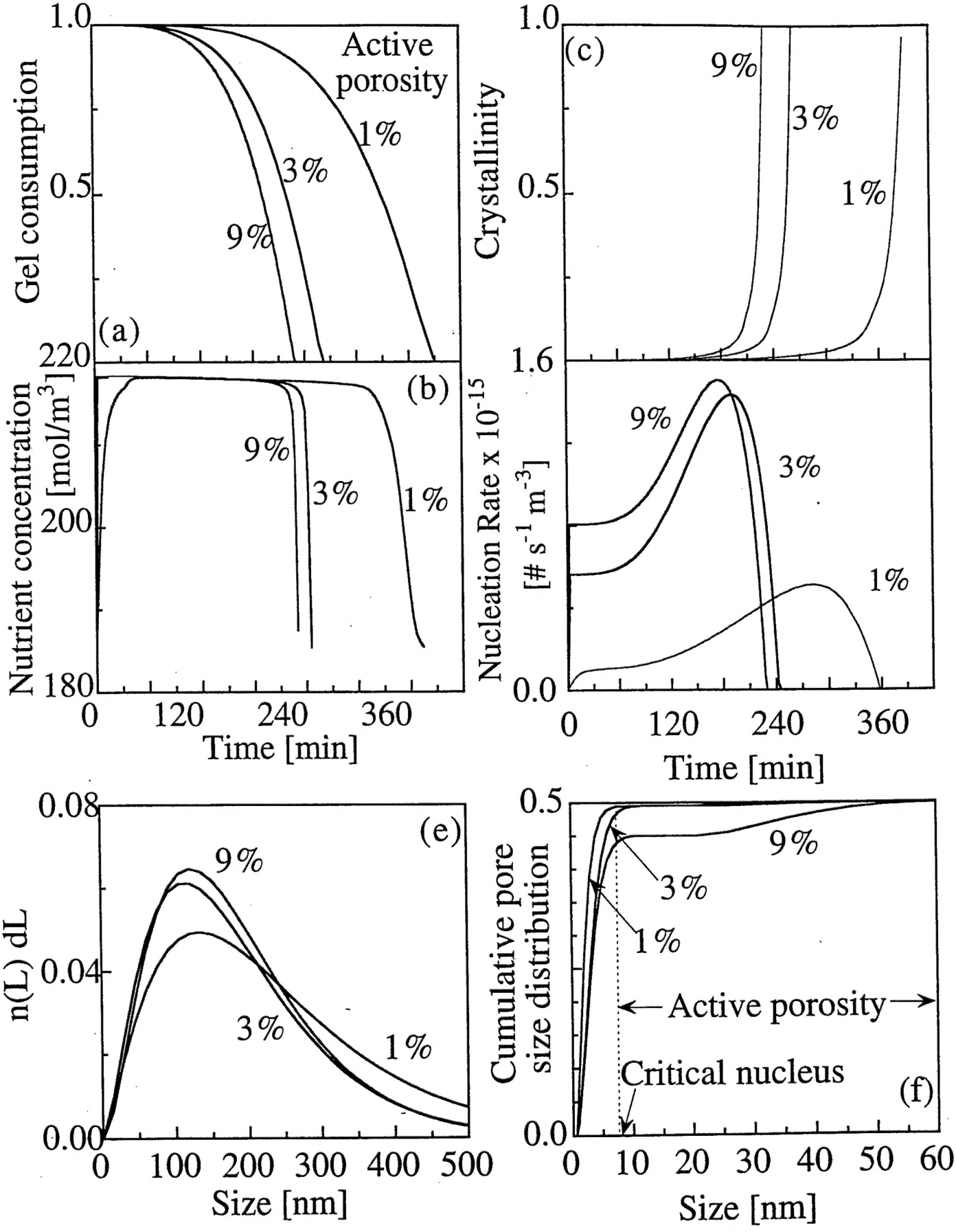

Figure 6, Nikolakis et al.